Oxidative and Tribological Properties of Amorphous and Quasicrystalline Approximant Al−Cu−Fe Thin Films

D. M. Rampulla, C. M. Mancinelli, I. F. Brunell, and A. J. Gellman*

Department of Chemical Engineering, Carnegie Mellon University, 5000 Forbes Avenue, Pittsburgh, Pennsylvania 15213

Received December 15, 2004. In Final Form: February 17, 2005

The origins of the tribological properties and corrosion resistance of amorphous and quasicrystalline approximant alloys have been studied by comparing their properties in thin Al−Cu−Fe alloy films with compositions lying near the quasicrystalline region of the ternary compositional phase diagram. Six sputtered thin films of an Al−Cu−Fe alloy were studied using X-ray diffraction, X-ray photoemission spectroscopy (XPS), and an in situ ultrahigh vacuum (UHV) tribometer. The films were annealed in UHV to induce the formation of orthorhombic, rhombohedral, and amorphous bulk structures. The properties of these thin films were then determined in the same UHV apparatus without exposing the films to air. The rates of surface oxidation by H_2O and O_2 were measured using XPS. Although the oxidation rates and oxide thicknesses were dependent on the oxidant, they were not sensitive to the structures of the films. Friction was measured between identical samples in sliding contact. The friction coefficients ($\mu_s = 0.36 \pm 0.11$ to 0.56 ± 0.08) were comparable to those observed in other experiments using quasicrystals and approximants in UHV; however, there was no strong correlation between the friction coefficients and either the film structure or the degree of surface oxidation. These results suggest that the tribological and corrosion resistance properties of these quasicrystalline approximant alloys are not directly connected to crystalline structure.

1. Introduction

In 1982 a new class of materials was discovered that possess long-range order but lack the translational periodicity of crystalline solids.[1,2] These new materials are called quasicrystals. Most quasicrystals are ternary or higher order metallic alloys that contain aluminum. Two common examples are $Al_{70}Pd_{21}Mn_9$ and $Al_{62}Cu_{26}Fe_{12}$. Since their discovery, quasicrystals have been studied extensively and found to possess interesting and potentially useful properties such as high hardness, low surface energy, high wear resistance, low friction, and resistance to oxidation.[3−18] One of the interesting scientific questions raised by these observations is the extent to which these properties arise directly from the quasicrystalline structure. Ideally, one would address this issue by comparing the properties of two alloys having identical compositions but different structures, one crystalline and the other quasicrystalline. This is, of course, difficult to achieve and so, comparisons have to be made between samples with varying composition.

The phase diagrams of the ternary alloys that form quasicrystals can be very complex. The quasicrystalline structure is, of course, only found over a narrow range of compositions. In the region immediately surrounding the quasicrystal region of the compositional phase diagram one finds the quasicrystal approximants. These have compositions close to those of the quasicrystal and structures that are related to those of the quasicrystal but are crystalline in the sense that they have long-range periodicity.[19−24] Because quasicrystals are close in com-

* Corresponding author. Tel.: 412-268-3848. E-mail: gellman@cmu.edu.

(1) Shechtman, D.; Blech, I.; Gratias, D.; Cahn, J. W. *Phys. Rev. Lett.* **1984**, *53*, 1951−1953.
(2) Shechtman, D.; Lang, C. I. *MRS Bull.* **1997**, *22*, 40−42.
(3) Chang, S. L.; Anderegg, J. W.; Thiel, P. A. *J. Non-Cryst. Solids* **1996**, *195*, 95.
(4) Demange, V.; Anderegg, J. W.; Ghanbaja, J.; Machizaud, F.; Sordelet, D. J.; Besser, M.; Thiel, P. A.; Dubois, J. M. *Appl. Surf. Sci.* **2001**, *173*, 327−338.
(5) Dubois, J. M.; Kang, S. S.; von Stebut, J. *J. Mater. Sci. Lett.* **1991**, *10*, 537−541.
(6) Dubois, J. M.; Kang, S. S.; Perrot, A. *Mater. Sci. Eng., A* **1994**, *179/A180*, 122−126.
(7) Gavatz, M.; Rouxel, D.; Pigeat, P.; Weber, B.; Dubois, J. M. *Philos. Mag. A* **2000**, *80*, 2083.
(8) Jenks, C. J.; Pinhero, P. J.; Chang, S. L.; Anderegg, J. W.; Besser, M. F.; Sordelet, D. J.; Thiel, P. A. Surface Oxidation of Al-Pd-Mn and Al-Cu-Fe Alloys. In *New Horizons in Quasicrystal Research and Applications*; Goldman, A. I., Sordelet, D. J., Thiel, P. A., Dubois, J. M., Eds.; World Scientific Publishing: Singapore, 1997; pp 157−164.
(9) Kang, S. S.; Dubois, J. M.; von Stebut, J. *J. Mater. Res.* **1993**, *8*, 2471−2481.
(10) Ko, J. S.; Gellman, A. J.; Jenks, C.; Lograsso, T.; Thiel, P. A. *Surf. Sci.* **1999**, *423*, 243−255.
(11) Pinhero, P. J.; Anderegg, J. W.; Sordelet, D. J.; Besser, M. F.; Thiel, P. A. *Philos. Mag. B* **1999**, *79*, 91.
(12) Pinhero, P. J.; Sordelet, D. J.; Anderegg, J. W.; Brunet, P.; Dubois, J. M.; Thiel, P. A. Room Temperature Oxidation of Al-Cu-Fe and Al-Cu-Fe-Cr Quasicrystals. *Mater. Res. Soc. Symp. Proc.* **1999**.
(13) Rouxel, D.; Gavatz, M.; Pigeat, P.; Weber, B.; Plaindoux, P. Auger Electron Microprobe Analysis of Surface of $Al_{62}Cu_{25.5}Fe_{12.5}$ Quasicrystal. First Steps of Oxidation. In *New Horizons in Quasicrystal Research*; Goldman, A. I., Sordelet, D. J., Thiel, P. A., Dubois, J. M., Eds.; World Scientific Publishing: Singapore, 1997; pp 173−180.
(14) von Stebut, J.; Soro, J. M.; Plaindoux, P.; Dubois, J. M. Friction Behavior of Pure Quasicrystalline Materials. In *New Horizons in Quasicrystals Research and Applications*; Goldman, A. I., Sordelet, D. J., Thiel, P. A., Dubois, J. M., Eds.; World Scientific Publishing: Singapore, 1997; pp 248−255.
(15) Wehner, B. I.; Köster, U. Oxidation Induced Phase Transformations in Al-Cu-Fe Quasicrystals and Crystalline μ-Al_5Fe_2. In *New Horizons in Quasicrystals Research and Applications*; Goldman, A. I., Sordelet, D. J., Thiel, P. A., Dubois, J. M., Eds.; World Scientific Publishing: Singapore, 1997; pp 152−156.
(16) Wehner, B. I.; Köster, U. Oxidation of Al-Cu-Fe Quasicrystals. *Mater. Res. Soc. Symp. Proc.* **1999**.
(17) Wehner, B. I.; Köster, U.; Rüdiger, A.; Pieper, C.; Sordelet, D. J. *Mater. Sci. Eng.* **2000**, *294−296*, 830−833.
(18) Wittmann, R.; Urban, K.; Schandl, M.; Hornbogen, E. *J. Mater. Res.* **1991**, *6*, 1165−1168.
(19) Quiquandon, M.; Calvayrac, Y.; Quivy, A.; Faudot, F.; Gratias, D. Phase diagrams and approximants. *Mater. Res. Soc. Symp. Proc.* **1999**.
(20) Menguy, N.; Audier, M.; Guyot, P.; Vacher, M. *Philos. Mag. B* **1993**, *68*, 595−606.
(21) Bancel, P. A. *Philos. Mag. Lett.* **1993**, *67*, 43−49.

10.1021/la0469093 CCC: $30.25
Published on Web 03/31/2005

position to approximants, mechanical stress and thermal activation can induce phase transitions in the quasicrystals that lead to the formation of approximant phases.[15,25−30]

Although quasicrystals have a number of useful properties their practical utility is limited by the fact that they are quite brittle. To circumvent this problem, methods have been developed to deposit thin quasicrystalline films on various substrate materials. This takes advantage of the high hardness and low friction of quasicrystal surfaces, while minimizing the effects of brittleness.[31] Because a cubic approximant is more thermally and mechanically stable than a quasicrystal, it should also produce a thin film with suitable properties.

One of the potentially important attributes of quasicrystals is their apparent resistance to oxidation. Studies of quasicrystal oxidation by exposure to O_2 have shown that a passivating aluminum oxide layer is formed on their surfaces preventing further oxidation of the bulk.[3,7,8,11−13,15,16,32,33] Upon exposure to H_2O (vapor or liquid), the oxide thickness has been shown to increase beyond the thickness obtained by O_2 exposure.[8] The passivating layer of aluminum oxide is formed by extraction of the Al from the near surface region of the alloy. The high heat of oxidation of the aluminum favors the formation of aluminum oxide over oxides of the other components of the quasicrystal alloy.[3,8,13,34−40] The formation of a passivating aluminum oxide film by segregation of Al results in depletion of the near surface region of the quasicrystal. The quasicrystalline phase typically occurs over a narrow range of Al concentrations. Hence, Al segregation to the surface during oxidation is particularly important because it could trigger a phase transformation that destroys the quasicrystalline structure of the near surface region.[15,32,41] Previous studies have addressed the connection between these oxidative properties and the quasicrystalline structure. They have shown that Al−Cu−Fe quasicrystals and their cubic approximants have similar oxidative properties and suggest that their resistance to oxidation is a result of the presence of Al in the alloy composition.[7,12]

The origin of the tribological properties of the quasicrystals and their approximants remains unclear. It has been suggested that the lack of periodicity of the quasicrystalline structure can lead directly to low friction coefficients during sliding. Many comparisons have shown that the quasicrystals have lower friction coefficients than most metals;[5,6,9,10,14,18,42−44] however, most such studies have been performed under conditions in which surface contamination can influence friction. Most studies have been performed in air and thus measured the frictional properties of surfaces that are coated with a thin oxide film. Careful studies of friction between pairs of $Al_{70}Pd_{21}Mn_9$ quasicrystal surfaces in ultrahigh vacuum (UHV) have shown that the friction between the truly clean surfaces is significantly higher than that between the air-exposed surfaces and that the presence of a thin oxide film does reduce friction.[10] There has been one attempt to compare the tribological properties of a quasicrystal and an approximant under the controlled conditions of UHV. That study made use of the $Al_{70}Pd_{21}Mn_9$ quasicrystal and an $Al_{48}Pd_{42}Mn_{10}$ approximant.[45,46] Those measurements suggest that the friction between the perfectly clean quasicrystalline surfaces is roughly half that of the approximant surfaces. The limitation in the interpretation of that study is that the composition of the $Al_{48}Pd_{42}Mn_{10}$ approximant is quite different from that of the $Al_{70}Pd_{21}Mn_9$ quasicrystal. Ideally, an investigation of the origins of the tribological properties of the quasicrystals would make use of a set of alloys with compositions that lie in and around the quasicrystalline region of the compositional phase diagram. Any structural dependence of the properties would be revealed by a change in their magnitude as the composition crosses the phase boundary.

The work reported in this paper has made use of six sputtered thin films with compositions in and around the quasicrystalline region of the phase diagram. Two samples were rhombohedral cubic approximants, two were orthorhombic cubic approximants, and two were amorphous. After verification of the bulk structures, the surfaces of these films were cleaned in UHV. Surface oxidation rates and friction coefficients of the thin films were then measured without exposure of the samples to ambient conditions. Our study of these thin films in an UHV environment has allowed precise control of the oxidation conditions and control of the surface characteristics prior to friction measurements.

2. Experimental Section

This study was conducted in two UHV chambers and an off-site X-ray diffraction laboratory. The alloy thin films deposited

(22) Gratias, D.; Calvayrac, Y.; Devaud-Rzepski, J.; Faudot, F.; Harmelin, M.; Quivy, A.; Bancel, P. A. *J. Non-Cryst. Solids* **1993**, *153−154*, 482−488.
(23) Waseda, A.; Araki, K.; Kimura, K.; Ino, H. *J. Non-Cryst. Solids* **1993**, *153−154*, 635−639.
(24) Fournee, V.; Ross, A. R.; Lograsso, T. A.; Anderegg, J. W.; Dong, C.; Kramer, M.; Fisher, I. R.; Canfield, P. C.; Thiel, P. A. *Phys. Rev. B: Condens. Matter* **2002**, *66*, 165423/1−165423/10.
(25) Dong, C.; Wu, J.; Zhang, L. M.; Dubois, J. M.; Brunet, P.; Zhou, Q. G.; Wang, D.; Zhang, H. C. Phase Transitions in Quasicrystals Induced by Friction and Wear. *Mater. Res. Soc. Symp. Proc.* **2001**.
(26) Shen, Z.; Kramer, M. J.; Jenks, C. J.; Goldman, A. I.; Lograsso, T.; Delaney, D.; Heinzig, M.; Raberg, W.; Thiel, P. A. *Phys. Rev. B: Condens. Matter* **1998**, *58*, 9961−9971.
(27) Wu, J. S.; Brien, V.; Brunet, P.; Dong, C.; Dubois, J. M. *Philos. Mag. A* **2000**, *80*, 1645.
(28) Beeli, C.; Horiuchi, S. *Philos. Mag. B* **1994**, *70*, 215−240.
(29) Dong, C.; Dubois, J. M.; Kang, S. S.; Audier, M. *Philos. Mag. B* **1992**, *65*, 107−126.
(30) Zhang, Z.; Feng, Y. C.; Williams, D. B.; Kuo, K. H. *Philos. Mag. B* **1993**, *67*, 237−251.
(31) Dubois, J. M.; Weinland, P. Coating material for aluminum alloys. In *Fr. Demande*; Centre National de la Recherche Scientifique, France: France, 1990; pp 23.
(32) Kang, S. S.; Dubois, J. M. *J. Mater. Res.* **1995**, *10*, 1071.
(33) Thiel, P. A.; Goldman, A. I.; Jenks, C. J. *Springer Ser. Solid-State Sci.* **1999**, *126*, 327−359.
(34) Gavatz, M.; Rouxel, D.; Claudel, D.; Pigeat, P.; Weber, B.; Dubois, J. M. *Quasicrystals, Proceedings of the International Conference, 6th*; Tokyo, May 26−30, 1997; 1998; pp 765−768.
(35) Jenks, C.; Pinhero, P. J.; Bloomer, T. E.; Anderegg, J. W.; Thiel, P. A.*Quasicrystals, Proceedings of the International Conference, 6th*; Tokyo, May 26−30, 1997; 1998.
(36) Chang, S. L.; Chin, W. B.; Zhang, C. M.; Jenks, C. J.; Thiel, P. A. *Surf. Sci.* **1995**, *337*, 135−146.
(37) Suzuki, S.; Waseda, Y.; Tamura, N.; Urban, K. *Scr. Mater.* **1996**, *35*, 891−895.
(38) Chevrier, J.; Cappello, G.; Comin, F.; Palmari, J. P. *New Horizons in Quasicrystals: Research and Applications, [Conference]*; Ames, IA, Aug. 19−23, 1996; 1997; pp 144−151.
(39) Gu, T.; Goldman, A. I.; Pinhero, P.; Delaney, D. *New Horizons in Quasicrystals: Research and Applications, [Conference]*; Ames, IA, Aug. 19−23, 1996; 1997; pp 165−168.
(40) Pinhero, P. J.; Chang, S. L.; Anderegg, J. W.; Thiel, P. A. *Philos. Mag. B* **1997**, *75*, 271−281.
(41) Sordelet, D. J.; Gunderman, L. A.; Besser, M. F.; Akinc, A. B. *New Horizons in Quasicrystals: Research and Applications, [Conference]*; Ames, IA, Aug. 19−23, 1996; 1997; pp 296−303.
(42) von Stebut, J.; Strobel, C.; Dubois, J. M. *Quasicrystals, Proceedings of the International Conference, 5th*; Avignon, May 22−26, 1995; 1995; pp 704−713.
(43) Kim, D. E.; Suh, N. P. *Wear* **1993**, *162−164*, 873−879.
(44) Rabinowicz, E. *Wear* **1992**, *159*, 89−94.
(45) Mancinelli, C.; Ko, J. S.; Jenks, C. J.; Thiel, P. A.; Ross, A. R.; Lograsso, T. A.; Gellman, A. J. *Mater. Res. Soc. Symp. Proc.* **2001**, *643*, K8.2.1−K8.2.10.
(46) Mancinelli, C.; Jenks, C. J.; Thiel, P. A.; Gellman, A. J. *J. Mater. Res.* **2003**, *18*, 1447−1456.

Table 1. Deposition Conditions and Film Structures for the Various Samples Studied

sample	target power (W)	substrate bias (V)	pressure (mTorr)	substrate−target distance (in.)	alloy composition	phase
1064	600	0	5	2.5	$Al_{63}Cu_{19}Fe_{18}$	rhombohedral
1065	600	0	5	2.5	$Al_{62}Cu_{20}Fe_{18}$	rhombohedral
1067	600	−25	5	2.5	$Al_{63}Cu_{19}Fe_{18}$	orthorhombic
1068	600	−75	5	2.5	$Al_{59}Cu_{17}Fe_{24}$	orthorhombic
1069	600	0	5	3.5	$Al_{72}Cu_{18}Fe_{10}$	amorphous
1070	600	0	10	2.5	$Al_{61}Cu_{28}Fe_{11}$	amorphous

on Ni substrates were mounted on manipulators that allowed sample motion within the UHV chambers and allowed heating and cooling of the samples over a temperature range of 100−1000 K. Both UHV chambers were equipped with Ar^+ ion guns for cleaning the surfaces of the alloy thin films. One UHV chamber was equipped to perform X-ray photoemission spectroscopy (XPS) with a Vacuum Generators (VG) Mg Kα X-ray source and a SPECS Lab PHOIBOS 150MCD hemispherical analyzer. XPS was used to determine the elemental composition of the alloy thin films in vacuo before and after cleaning by Ar^+ ion bombardment and annealing. In addition, XPS was used to measure the uptake of oxygen on the surfaces following exposures to O_2 and to H_2O vapor. The second UHV chamber was equipped with a tribometer that was used to make friction measurements between pairs of identical films. A detailed description of the tribometer has been given elsewhere.[47] The crystal structures of the thin films were determined by X-ray diffraction (XRD) using a Rigaku X-ray diffractometer.

All samples were obtained from Technology Assessment & Transfer, Inc. (TA&T, located in Annapolis, MD). The Al−Cu−Fe films were deposited on a nickel foil substrate by magnetron sputtering using an Al−Cu−Fe target. The films were sputtered under a variety of conditions to produce a range of different compositions around those of the $Al_{62}Cu_{26}Fe_{12}$ quasicrystal.[48] The samples were numbered and Table 1 shows the sputtering conditions used to obtain each sample. Al−Cu−Fe films with a thickness of roughly 1 μm were deposited on a single sheet of 0.5 mm thick Ni foil. Two 1 cm diameter disks were punched from each of these foils and were used throughout the study.

In both the XPS chamber and the tribometry chamber the samples were mounted on manipulators allowing *xyz* motion and rotation about the vertical axis of the chamber. The samples were spot-welded between two Ta wires and could be heated resistively to $T > 1000$ K and cooled to $T < 100$ K through mechanical contact with a liquid nitrogen reservoir. The temperature of the samples was measured using a K-type thermocouple spot-welded to the back of the nickel foil.

Once mounted in the UHV chamber the as-received samples were cleaned by Ar^+ ion bombardment to remove oxygen and other surface contaminants. The cleanliness of the samples was then determined using XPS. After surface cleaning, the samples were annealed at 720 K for 2.5 h in a vacuum of $< 10^{-9}$ Torr to induce a phase transition from the amorphous as-sputtered structure to the stable phase. An XPS spectrum was taken after annealing to determine the elemental composition of the sample surface and to determine its location in the compositional phase diagram.

The cleaned and annealed samples were systematically oxidized and XPS was used to monitor the uptake of oxygen. During oxidation, the samples were held at 300 K. XPS spectra were obtained after each exposure to O_2 with the total exposure reaching 64 L. For O_2 exposures of 1, 2, and 4 L the background pressure was 1×10^{-8} Torr. For O_2 exposures of 8 and 16 L the background pressure was 2×10^{-8} Torr. For O_2 exposure of 32 L the background pressure was 4×10^{-8} Torr, and for 64 L the background pressure was 8×10^{-8} Torr. Higher pressures were used for higher exposures to allow shorter exposure times, reducing surface contamination. The samples were cleaned by Ar^+ sputtering after oxidation in O_2 and prior to oxidation in H_2O. Oxidation of the surfaces in H_2O was performed using a series of exposures totaling 2 L. For H_2O exposures of 0.2 L, 0.4 L, 0.6, 0.8, and 1 L the background pressure was 8×10^{-9} Torr, and for exposures of 1.5 and 2 L the background pressure was 1×10^{-8} Torr. Again a higher pressure was used for higher exposures to minimize exposure times and thus reduce contamination. Maximum exposures of 64 L for O_2 and 2 L for H_2O were chosen, because these exposures were sufficient to saturate the oxide film. After each exposure of the surface to either O_2 or H_2O an XPS spectra was taken to monitor the change in O 1s, Al 2p, Fe $2p_{3/2}$, and Cu $2p_{3/2}$ peaks. Spectra that covered a large range of binding energies were taken with a dwell time of 0.1 s, while spectra that covered a narrow range of binding energies to more closely examine single peaks were taken with a dwell time of 1 s. The X-ray source was operated at 600 W and induced a photoemission current of ∼100 nA from the sample. The instrumental resolution, measured as the fwhm for the Al 2p peak, was 1.5 eV at a pass energy of 25 eV.

After completion of the surface oxidation measurements, the samples were removed from the XPS chamber and moved to the XRD system to determine the structures of the films. Pairs of identical samples were then mounted in the UHV tribometry chamber.

Friction measurements between pairs of the films were made in the UHV tribometry chamber.[47] One sample was pressed between two curved watch glasses to give it a slight curvature, while the other sample remained flat. This allows the two to be brought into contact while avoiding contact at the edges. The curved sample was mounted on the manipulator while the flat sample was mounted to the UHV tribometer. Both samples were mounted in place by spot-welding to Ta wires and both had thermocouples attached to them. In the tribometry chamber the samples could be cooled to ∼100 K and heated to ∼800 K. They were cleaned using the same treatment as was used prior to the XPS measurements (i.e., Ar^+ ion bombardment and annealing to 720 K). Friction measurements were made between pairs of clean surfaces and between surfaces that had been subjected to controlled oxidation treatments similar to those used in the oxygen uptake experiments. During each friction measurement, the samples were held at 300 K. A normal force of 60 mN and a sliding speed of 20 μm/s were used. To obtain statistically meaningful data a total of 12 friction measurements were made between each pair of films under each set of conditions. Between measurements the samples were moved relative to one another to ensure that new contacts were formed between fresh surfaces.

The film surfaces were oxidized by systematic background exposure to extra-dry O_2 (Matheson Purity, 99.997%) or purified H_2O vapor. All exposures are reported in units of Langmuirs (1 L = 10^{-6} Torr·s) with the pressure uncorrected for ion gauge sensitivity.

3. Results and Discussion

3.1. Alloy Film Structure. XRD measurements were used to determine the bulk structures of the annealed Al−Cu−Fe films. Figure 1 shows the three types of diffraction patterns obtained from the XRD measurements. These diffraction patterns were compared to existing XRD patterns that exhibit signatures of the three crystalline phases. Two films had rhombohedral structures (1064 and 1065), two films had orthorhombic structures (1067 and 1068), and two films were amorphous (1069 and 1070). All three XRD patterns exhibit diffraction peaks attributed to Ni located at 52° and 77°. Centered at ∼43° are peaks that are attributed to the alloy. For sample 1070 the diffraction shows a large featureless peak at

(47) Gellman, A. J. *J. Vac. Sci. Technol. A* **1992**, *10*, 180.
(48) Quiquandon, M.; Quivy, A.; Devaud, J.; Faudot, F.; Lefebvre, S.; Bessiere, M.; Calvayrac, Y. *J. Phys.: Condens. Matter* **1996**, *8*, 2487−2512.

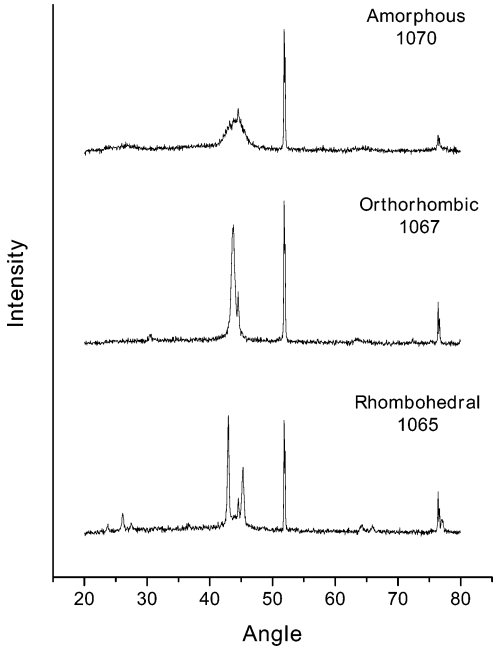

Figure 1. X-ray diffraction patterns for Al−Cu−Fe films with amorphous, orthorhombic, and rhombohedral structures. The amorphous film is indicated by a wide peak at ~43°. The orthorhombic and rhombohedral diffraction patterns have sharp peaks indicating crystalline Al−Cu−Fe alloys.

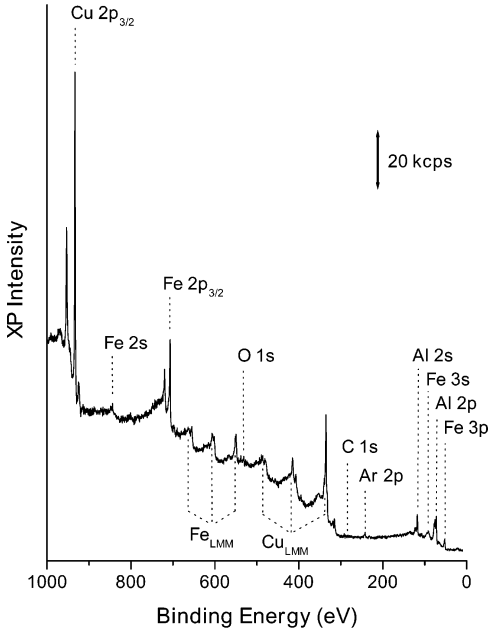

Figure 2. Wide scan XPS spectrum of sample 1065 showing the assignments of all X-ray photoemission and Auger peaks. There is a small amount of residual oxygen on the surface and almost no carbon.

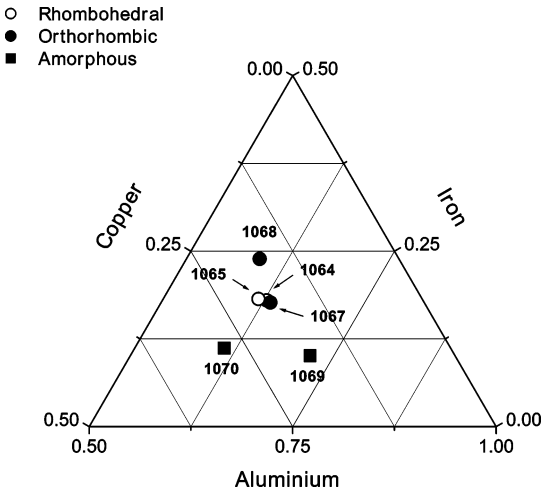

Figure 3. Ternary compositional phase diagram showing the rhombohedral (○), orthorhombic (●), and amorphous (■) phases. Despite the narrow range of film compositions, three distinct phases were created during annealing.

~43°, indicative of an amorphous structure. The orthorhombic and rhombohedral spectra were compared to previous XRD spectra for verification. The orthorhombic structure (1067) is identified by one large peak near 43°, and the rhombohedral structure (1065) is identified by three small peaks between 20° and 30° and two large peaks near 43° and 45°.[49] The rhombohedral structure is similar to an icosahedral quasicrystalline structure; thus, their spectra are quite similar. The rhombohedral XRD exhibits a small degree of peak splitting and broadening in the peaks between 20° and 30° that would not be present in the XRD of a quasicrystal.[23]

3.2. Alloy Film Composition. XPS was used to determine the elemental composition of the Al−Cu−Fe films. The film surfaces were cleaned by cycles of Ar^+ bombardment and annealing until the signal from the O 1s photoemission peak could not be reduced further. The residual oxygen was believed to be diffusing to the surface from the bulk of the film during annealing. While oxygen was never completely removed from the film, it was reduced to < 10% of the total composition of the sample. The XPS spectrum of sample 1065 in Figure 2 shows that the residual oxygen at the surface is negligible compared to the other components of the film. Once the surface oxygen concentration had been reduced to a minimum for each of the films, their XPS spectra were analyzed to determine their elemental compositions. The areas under the peaks for Al 2p, Fe $2p_{3/2}$, and Cu $2p_{3/2}$ were scaled by the sensitivity factors 0.25, 2.91, and 3, respectively, to determine relative amounts of Al, Cu, and Fe. The film compositions are plotted on the Al−Cu−Fe ternary phase diagram in Figure 3.

The rhombohedral films have a narrow range of compositions, while the orthorhombic and amorphous films vary considerably. The orthorhombic films have two different compositions. One film is Fe rich and has a composition very different from all of the other films. The composition of the other orthorhombic film (1067) is extremely close to the compositions of the other rhombohedral films. For film 1067 a negative bias of −25 V was applied to the substrate during deposition. This slight change in processing parameters resulted in a film that annealed to produce an orthorhombic structure although its composition was very close to that of the rhombohedral approximant. The fact that this film did not anneal into the rhombohedral structure may simply be a reflection of the uncertainty in the composition or that deposition parameters affect the structure during film growth.

3.3. Oxidation of Al−Cu−Fe Surfaces. The Al−Cu−Fe films were oxidized by exposure to O_2 and to H_2O vapor. The uptake of oxygen on the surfaces was determined using XPS. Exposure of the Al−Cu−Fe films to oxidizing environments selectively oxidized the Al to form a passivating layer of Al_2O_3. Figure 4 shows the evolution of the O 1s and Al 2p XPS peaks of the rhombohedral film 1065 following increasing exposure to oxygen. The O 1s

(49) Daniels, M. J. K. D.; Fehrenbacher, L.; Zabinski, J. S.; Bilello, J. C. *Surf. Coat. Technol.* **2005**, *191* (1), 96−101.

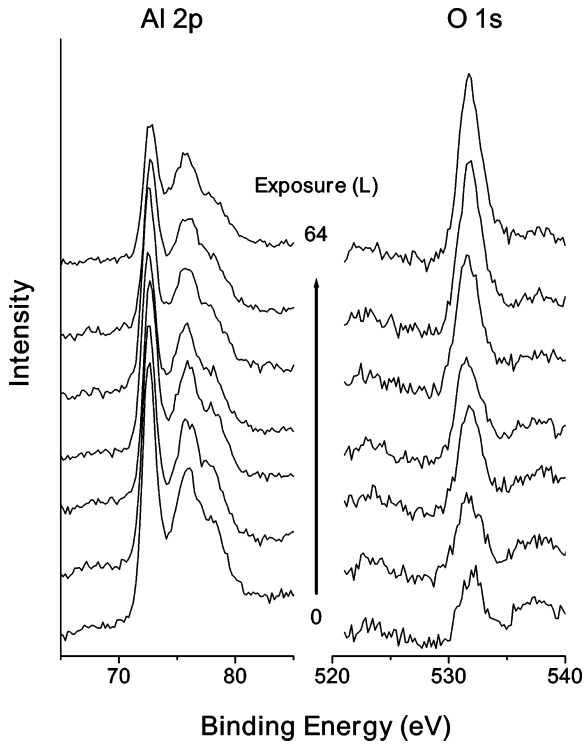

Figure 4. O 1s and Al 2p XPS spectra from the Al−Cu−Fe film surface (1065) during exposure to O_2. The O 1s peak increases in intensity with increasing exposure. The increase in intensity of the peak located at 76 eV is indicative of formation of the passivating Al_2O_3 overlayer, which causes a change in Al 2p peak shape.

peak increases in intensity with increasing exposure. The presence of a small O 1s peak at the beginning of the experiment reveals the fact that it was not possible to get the surface perfectly clean by sputtering. The Al 2p peak (73 eV) changes shape as a result of the growth of a second peak (76 eV), which is indicative of Al_2O_3 growth.[4] The Al_2O_3 film on the Al−Cu−Fe surface is formed by segregation of the Al from the near surface bulk. This Al_2O_3 film attenuates photoemission from the Al−Cu−Fe bulk. Figure 5 shows the attenuation of the Fe $2p_{3/2}$ and the Cu $2p_{3/2}$ photoemission peaks during oxidation of the rhombohedral film 1065. No oxidation of Fe or Cu was detected. The oxidation of all six alloy films during exposure to O_2 at 300 K was studied using XPS. There were no differences in the qualitative aspects of the oxidation of the six alloy surfaces used in this work. All six formed passivating films of Al_2O_3, and there was no evidence of the oxidation of either Fe or Cu.

The oxidation kinetics of the Al−Cu−Fe surfaces was monitored using XPS to measure the uptake of oxygen as a function of exposure to O_2 or H_2O at 300 K. An oxygen uptake curve measured on sample 1064 is shown in Figure 6. This curve is representative of the uptake curves for the other films. A small amount of oxygen was always present on the film surfaces even after extensive cleaning; therefore, the experiments could not be initiated with perfectly clean surfaces. During exposure to O_2 the oxide coverage rises rapidly at low exposures and then saturates at higher exposures. Saturation occurs as a result of the passivation of the surface with a thin film of Al_2O_3. The initial oxidation rate was obtained from the initial slope of the oxide coverage versus exposure curve, which was found by fitting a straight line through the low exposure region. The rates of oxidation by O_2 or H_2O were determined for each film and are compared in Figure 7.

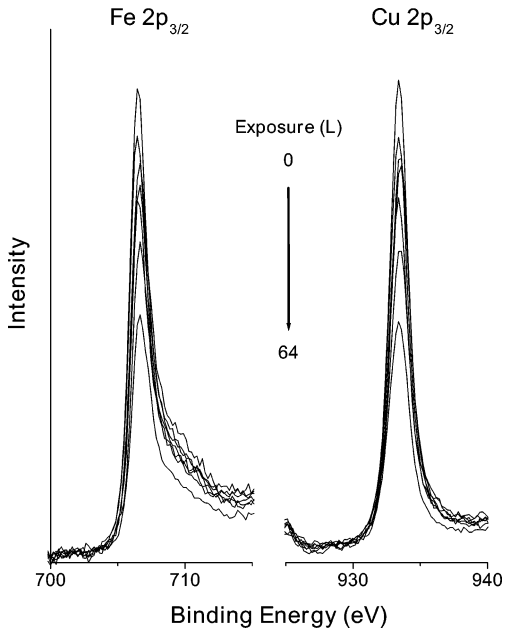

Figure 5. Cu $2p_{3/2}$ and Fe $2p_{3/2}$ XPS spectra from the Al−Cu−Fe film surface (1065) obtained following increasing exposures to O_2. The Cu $2p_{3/2}$ and Fe $2p_{3/2}$ peaks are both attenuated during increasing exposure to O_2 as a result of the growth of the passivating Al_2O_3 overlayer.

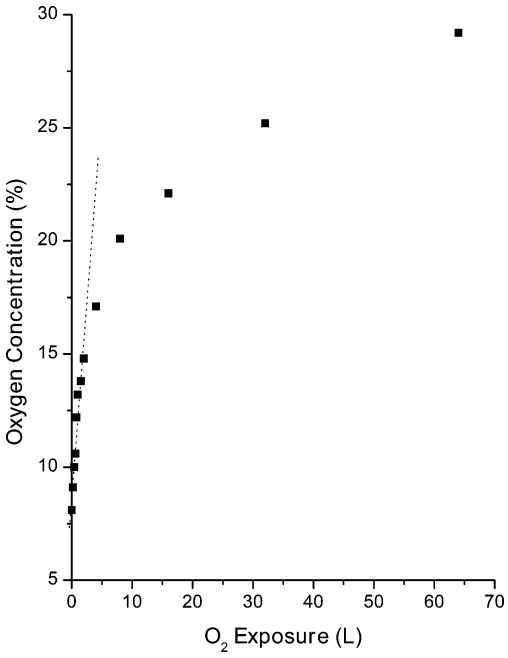

Figure 6. Increase in the oxygen concentration on the Al−Cu−Fe film surface (1064) as a function of exposure to O_2. The initial rate of oxidation is relatively high and then decreases as the surface is passivated with a thin film of Al_2O_3.

For all films the rate of oxidation by H_2O vapor was significantly higher than the rate of oxidation by O_2. Although the oxidation rates depend on the oxidant, there is no strong correlation between the oxidation rates and film structure. The only indication of correlation may be in the initial oxidation rates in the presence of H_2O, which are roughly twice as high on the rhombohedral phase as on the orthorhombic phase. The oxidation rates differ by less than a factor of 2 among the different films.

The thicknesses of the saturated oxide films formed by oxidation with O_2 and H_2O vapor were determined for each film. The asymptotic values of the O 1s XPS signal

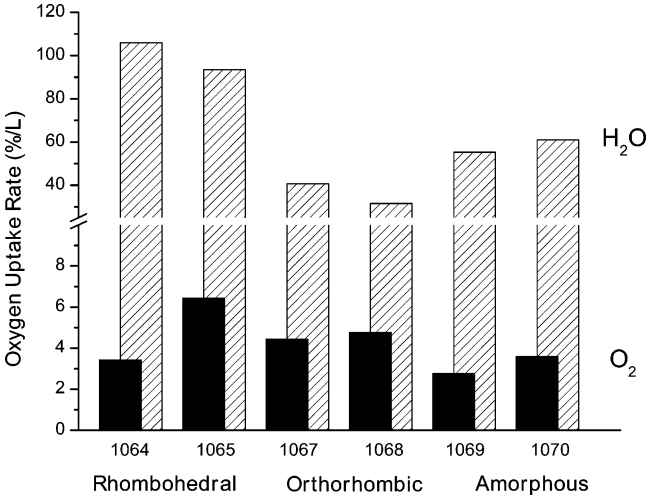

Figure 7. Initial oxygen uptake rates for each Al−Cu−Fe film during exposure to dry O_2 (solid bars) and H_2O vapor (hatched bars) at 300 K. The rates of oxidation during exposure to H_2O vapor are 10 to 30 times higher than the oxidation rates during exposure to O_2.

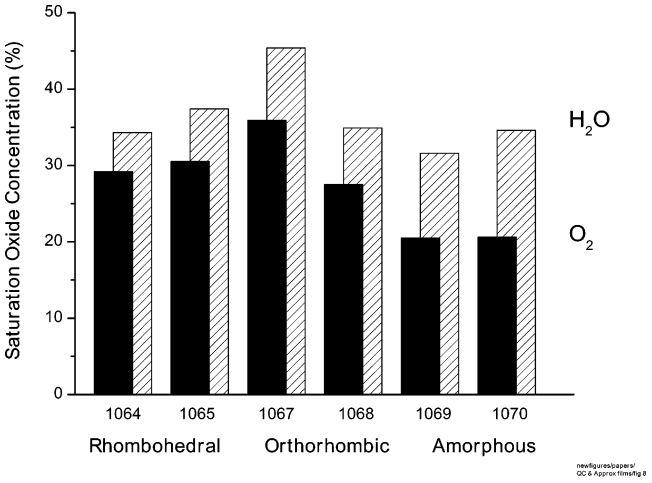

Figure 8. Saturation oxide thickness on each Al−Cu−Fe film during exposure to dry O_2 (solid) and H_2O vapor (hatched) at 300 K. The oxide is thicker following exposure to H_2O vapor than following exposure to O_2.

were used as a measure of the oxide thickness and are shown in Figure 8. In all cases, exposure to H_2O vapor produced a thicker oxide film than exposure to O_2. This is in agreement with previous comparisons of quasicrystal approximant oxidation by O_2 and H_2O.[4,11] Although the saturation oxide thickness depends on the oxidant, the thicknesses were all approximately the same regardless of the film structure. Previous studies show that Al concentration dictates oxidation kinetics, thus there is little difference in the thicknesses of the Al_2O_3 films produced on rhombohedral and orthorhombic structures with similar compositions.[11]

3.4. Friction between Al−Cu−Fe Surfaces. A UHV tribometer was used to measure friction between the surfaces of identical pairs of Al−Cu−Fe samples. Figure 9 shows three plots of single-pass friction measurements between clean rhombohedral Al−Cu−Fe films (1064). The plots show the normal and shear forces as a function of time before, during, and after the samples were brought into sliding contact. The friction forces between the rhombohedral films indicate fairly smooth sliding without any stick−slip behavior. The frictional behavior of interfaces between the surfaces of clean orthorhombic Al−Cu−

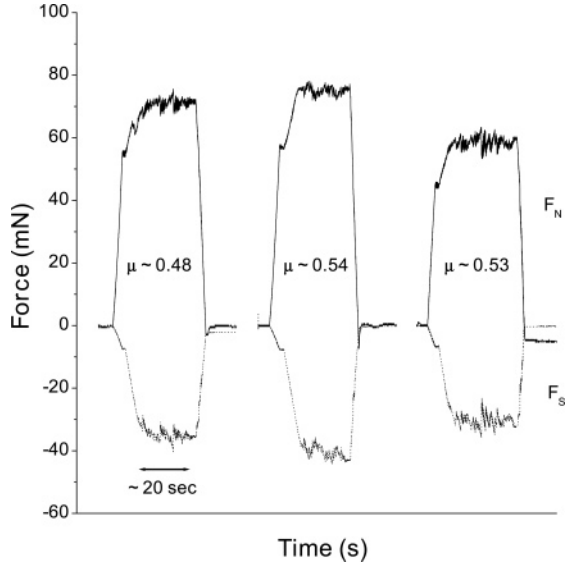

Figure 9. Plots of shear and normal forces (F_S and F_N) between two clean surfaces of an Al−Cu−Fe film (1064) during sliding. Sliding conditions were $T = 300$ K, $F_N = 60$ mN, and $v_s = 20$ μm/s.

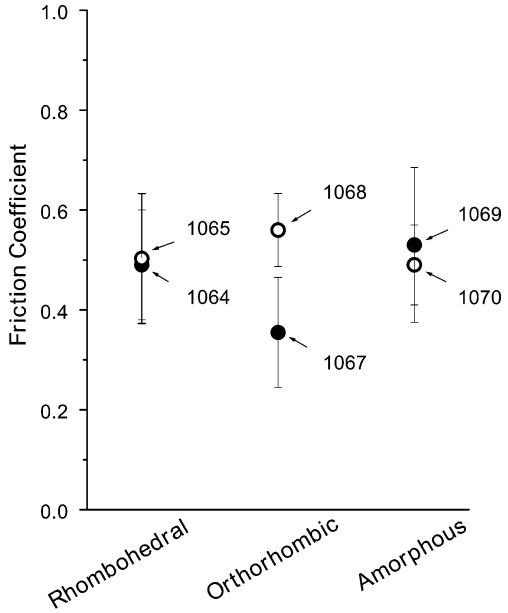

Figure 10. Static friction coefficients between clean surfaces of different Al−Cu−Fe films. The friction coefficients exhibit no significant structure dependence. Sliding conditions were $T = 300$ K, $F_N = 60$ mN, and $v_s = 20$ μm/s.

Fe films and interfaces between the surfaces of clean amorphous Al−Cu−Fe films was similar to that illustrated in Figure 9, although there was a small amount of stick−slip behavior between the orthorhombic films. Adhesion would manifest itself in a negative normal force during separation of the samples but was not observed during separation of any of the pairs of samples.

For each of the six alloy films, static coefficients of friction were estimated from 12 independent measurements of friction made at different points on the films' surfaces. The static coefficients of friction between the clean surfaces of the six different films are plotted in Figure 10 and appear to be independent of structure. The error bars denote one standard deviation estimated from 12 separate measurements of friction. The sample labeled 1067 has lower friction than the rest in both the clean and oxidized state. It also appears to have a thicker oxide film.

There is no relationship, however, between oxide film thickness and friction for the other films and so the origin of its lower friction coefficient is not clear. Numerous studies by Zhang et al. examined the friction coefficients of quasicrystal and approximant Al−Cu−Fe surfaces with nearly identical compositions.[50−52] They found that there is no statistically significant dependence of the friction on the structure of the bulk sample. There are several points to keep in mind in interpreting the friction measurements made in our study. The fact that the materials used in this study were thin alloy films on Ni substrates means that the contact area between the samples will to some extent be dictated by the hardness of the Ni substrate and not the properties of the thin films themselves. Other studies have measured friction between bulk crystalline samples and not thin films.[45,46,50] Thus the friction coefficients measured in this work may be dictated more by the surface properties of the films and less by their hardness than friction coefficients measured between bulk samples.

Friction measurements were made between oxidized surfaces of the Al−Cu−Fe alloy films to study the influence of surface oxidation on their tribological properties. Figure 11 shows the static friction coefficients measured using each of the completely oxidized films. Each point represents the static friction coefficient obtained by averaging the results of 12 friction measurements. These measurements reveal no significant change in the friction coefficients as a result of the oxidation of the surface. This result differs from those of previous studies using bulk Al−Pd−Mn alloys which revealed a decrease in friction, after oxidation, for both the quasicrystalline sample and an approximant sample,[10] and a study using Al−Cu−Fe alloys which revealed an increase in friction, after oxidation.[53] The fact that there is no significant change in the friction of the Al−Cu−Fe alloys as a result of oxidation may be due to the fact that in these measurements it was never possible to completely remove the oxide from the surface initially. Thus the comparison of the data in Figures 10 and 11 is not being made to the truly clean surface.

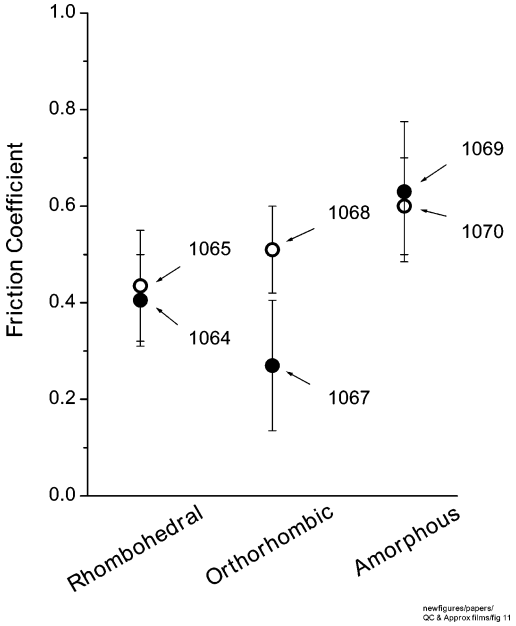

Figure 11. Static friction coefficients between oxidized surfaces of different Al−Cu−Fe films. The friction coefficients exhibit no significant structure dependence. The surface was completely saturated by successive exposures of O_2 (64 L) and H_2O (128 L). Sliding conditions were $T = 300$ K, $F_N = 60$ mN, and $v_s = 20$ μm/s.

4. Conclusions

A study has been conducted of the oxidation and tribological properties of a set of six Al−Cu−Fe films having compositions near that of the $Al_{62}Cu_{26}Fe_{12}$ quasicrystalline phase but structures that were amorphous, rhombohedral or orthorhombic. Oxidation was found to occur via the formation of a passivating Al_2O_3 overlayer. For each film, the oxidation rate during exposure to H_2O vapor was roughly 10 times higher than the oxidation rate during exposure to O_2. In addition the oxide films created by exposure to H_2O vapor were thicker than those created by exposure to O_2. The oxide thicknesses and oxidation rates do not appear to depend significantly on film composition or structure. These results are consistent with previous work on the oxidation of these types of alloys.[3,7,8,11−13,15,16,32,33] Friction measurements made between pairs of Al−Cu−Fe films showed that the friction coefficients measured for all the films are comparable to those observed using quasicrystals and approximants in UHV and that they are not significantly structure sensitive. Comparison of the friction measurements made using these thin films and those made using bulk quasicrystals and approximants is complicated by the fact that the thin films have been deposited on Ni, a softer substrate. Although there are some variations in the properties of the different films there is no apparent correlation to their structures.

Acknowledgment. We would like to acknowledge Technology Assessment & Transfer, Inc., for preparing and providing the Al−Cu−Fe thin film samples, and Dr. Matt Daniels for his helpful discussions. Funding for this work was provided by DARPA and the AFOSR through Grant AFOSR F49620-01-1-0069.

LA0469093

(50) Zhang, L. M.; Zhang, H. C.; Zhou, Q. G.; Dong, C. *Wear* **1999**, *225−229*, 784−788.
(51) Zhang, L. M.; Dong, C.; Brunet, P.; Dubois, J. M. *Mater. Sci. Eng., A* **2000**, *294−296*, 810−812.
(52) Zhang, L.-M.; Brunet, P.; Zhang, H.-C.; Dong, C.; Dubois, J.-M. *Tribol. Lett.* **2000**, *8*, 233−236.
(53) Dubois, J.-M.; Brunet, P.; Costin, W.; Merstallinger, A. *J. Non-Cryst. Solids* **2004**, *334/335*, 475−480.